Galvis, F. A., Hulsey, A. M., Baker, J. W., and Deierlein, G. G. (2023). "Simulation-Based Methodology to Identify Damage Indicators and Safety Thresholds for Post-Earthquake Evaluation of Structures." *Earthquake Engineering & Structural Dynamics*, (in press).

RESEARCH ARTICLE

Simulation-Based Methodology to Identify Damage Indicators and Safety Thresholds for Post-Earthquake Evaluation of Structures

Francisco A. Galvis*[1] | Anne M. Hulsey[2] | Jack W. Baker[3] | Gregory G. Deierlein[3]

[1]Thornton Tomasetti Inc., California, USA
[2]Department of Civil & Environmental Engineering, University of Auckland, Auckland, New Zealand
[3]Department of Civil & Environmental Engineering, Stanford University, California, USA

Correspondence
*Francisco A. Galvis Email: galvisf@alumni.stanford.edu

Abstract

After a strong earthquake, criteria are needed to determine whether buildings are safe to reoccupy based on observable damage. This paper presents a simulation-based methodology to identify relevant damage indicators and safety thresholds for building structures. Prior knowledge of the most relevant damage indicators and their thresholds can increase the accuracy and confidence of post-earthquake evaluations. Current practice to translate observable damage into a tagging decision relies on qualitative guidelines based on past earthquake experience and judgment, which may be susceptible to speculation and interpretation. In addition, past experience may not be relevant to newer structural systems and to large or complex (e.g., high-rise) buildings. To augment past observations and data from structural component tests, nonlinear dynamic analyses can be used to estimate the collapse safety of structures with simulated damage. Technologies to execute these simulations have matured over the years, although to date they have not been systematically applied to evaluate the destabilizing effects of simulated damage on collapse safety. In this paper, a methodology is presented to use numerical simulations of damage to identify and evaluate relevant damage indicators that can be quantitatively related to safety thresholds. Damage indicators are selected based on their reliability in estimating the structural safety and their sensitivity to modeling uncertainty, i.e., where the preferred indicators are insensitive to variability in the structural materials and model parameters. The safety threshold for each damage indicator is selected to maximize accuracy in post-earthquake building assessments. The methodology is demonstrated through an application study of ductile reinforced concrete frame buildings. Results show that aggregated indices of structural component damage (e.g., aggregated over the floor of a building) outperform other damage indicators based on peak or residual drifts or simpler percentages of damaged components. Subject to agreement of a number underlying assumptions, this methodology can be applied to a wider variety of structures to improve post-earthquake evaluation guidelines.

KEYWORDS:
post-earthquake safety, damage indicators, tagging, reinforced concrete frames

1 | INTRODUCTION

One of the first priorities following an earthquake is to ascertain whether structures are safe to reoccupy. The most widely used references to support such decisions are post-earthquake inspection and evaluation guidelines largely based on lessons learned from past earthquakes.[1,2,3] These guidelines provide qualitative criteria for classifying damaged structures as unsafe (red tag), safe (green tag), or restricted use (yellow tag) until a more detailed evaluation is performed. The guiding criterion in tagging a structure is an "unsafe structure", which in this context is often defined as one that poses "imminent risk of further damage or collapse from creep or aftershocks."[1] Under that definition, qualitative guidelines are effective for classifying structures that lack redundancy and have obvious flaws (e.g. soft-story buildings), because damage in a few components can significantly heighten the risk of further damage or collapse. However, structures with limited permanent displacement and moderate damage to many elements are difficult to evaluate using qualitative guidelines, which can result in erroneous tags or indecisive yellow tags.

Detailed evaluations following FEMA-306[4] for concrete and masonry wall buildings or FEMA-352[5] for welded steel moment frame buildings support more definitive decisions by specifying quantitative safety thresholds. However, the recommended thresholds in these guidelines are not tied to an explicit quantification of the collapse safety of damaged buildings, making it unclear how well the thresholds correlate to an increased risk of collapse. Furthermore, FEMA-306[4], and FEMA-352[5] are largely based on empirical evidence from past earthquakes, which suggests that they may overlook structural failure mechanisms that have either not been observed in past earthquakes or ignore new structural systems that have not experienced damaging earthquakes.

Recognizing the limitations of data from past earthquakes, a number of previous research studies have utilized nonlinear analysis models to quantify the collapse safety of structures with simulated earthquake damage. To facilitate the calculations, many of these studies relied on simplified single-degree-of-freedom (SDOF) models that do not explicitly capture the localized damage and details of the structural response. In one of the earliest of these studies, Bazzurro et al.[6] performed nonlinear response history analyses (NLRHA) of SDOF models subjected to sequences of two ground motions, where the first motion generated structural damage, and the second motion was scaled to an intensity that would collapse the damaged structure. In parallel, Luco et al.[7] used a similar approach to explore the effects of a damaging mainshock ground motion to evaluate the structural collapse safety to a subsequent aftershock. Maffei et al.[8] extended the use of SDOF models to quantify post-earthquake safety to various structural systems, and Iervolino et al.[9] developed a method to account for multiple aftershocks. While the SDOF model studies provide valuable understanding of the general response of structures under sequential ground motions, they do not provide the level of detail necessary to translate simulation results into practical recommendations that could be used in post-earthquake inspection and evaluation guidelines.

Advances in computational resources have allowed the use of more detailed models for damage and post-earthquake simulation of real structures.[10,11,12,13,14] Detailed models enable a better understanding of the damage patterns that can reduce collapse safety. For instance, Raghunandan et al.[11] used detailed models of RC frames to evaluate the effectiveness of alternative damage indicators for predicting the reduction in collapse capacity of damaged buildings. They found that the maximum story drift is the best damage indicator, closely followed by residual story drift and roof drifts. Their work was the first to systematically evaluate and rank a set of observable damage indicators that could inform safety decisions based on their correlation with the reduced collapse safety caused by structural damage. However, their study does not provide a way to select quantitative thresholds for the top-ranked damage indicators, nor does it consider the sensitivity of the damage indicators to modeling uncertainty.

Burton and Deierlein[15] proposed a methodology that builds upon the Raghunandan et al. approach to simulate building damage and quantify post-earthquake collapse safety. Two significant contributions of their study are (1) to establish the safety threshold of a damaged building with respect to its intact safety index, and (2) to establish a corresponding threshold value of an observable damage indicator to assess the acceptable safety limit. Zhang and Burton[16] and Zhang et al.[17] further explored this idea and developed machine learning algorithms to estimate the safety of damaged buildings based on several damage indicators.

In addition to the challenge of establishing an acceptable level of reduced safety for an earthquake-damaged building, the sensitivity of the proposed damage index to variations in the structural component properties and materials is an important consideration. The sensitivity of the damage indices to structural modeling uncertainty may limit the acceptance of the research results. From a practical standpoint, evaluations of existing buildings are faced with inherent limits on characterizing the quality of the structural components. Previous research has shown that variability in modeling parameters leads to bias and increases dispersion in collapse safety evaluations of intact structures.[18] This susceptibility to modeling uncertainty has likewise been shown to impact collapse evaluations of damaged structures.[19] Hence, it is crucial to explicitly consider modeling uncertainty when evaluating damage indicators and defining quantitative safety thresholds.

This paper presents a simulation-based methodology to identify relevant damage indicators and safety thresholds for building structures to facilitate post-earthquake occupancy decisions using detailed building inspections. The methodology advances concepts from previous studies[11,15] that use data from numerical simulations to select the most relevant damage indicators and identify safety thresholds for damaged structures. By focusing on the state of the building following the damaging earthquake, this study informs decisions by estimating the level of safety of a damaged structure compared to an intact building, rather than attempting to quantify the explicit collapse risk to mainshock-aftershock sequences. The proposed methodology considers a set of candidate damage indicators for a structure of interest, evaluating them in light of their ability to estimate the collapse safety once the structure is damaged, and the stability (or insensitivity) of the thresholds to modeling uncertainty. The safety threshold for the selected indicators is selected considering tipping points, where there is a rapid reduction in collapse safety with a small increment of damage. By searching for the point where there is a noticeable change in structural response, the approach sidesteps the otherwise tricky question of establishing an absolute acceptable safety limit. The proposed methodology is envisioned to enhance the reliability of detailed building evaluations, especially those assigned yellow tags after rapid building evaluations.

2 | STRUCTURAL DAMAGE AND POST-EARTHQUAKE DATA GENERATION

Referring to Figure 1, the process for generating simulation data to assess the safety of earthquake-damaged structures begins with the definition of structural models and a suite of ground motions. The structural models should be detailed enough to capture all possible failure modes of the structure of interest. The outputs of this process are a series of scalar damage indicators that measure the amount of structural damage (discussed in more detail in Section 2.1), and a scalar collapse risk metric, κ, that quantifies the collapse safety of a damaged structure with respect to its intact state (discussed in more detail in Section 2.2).

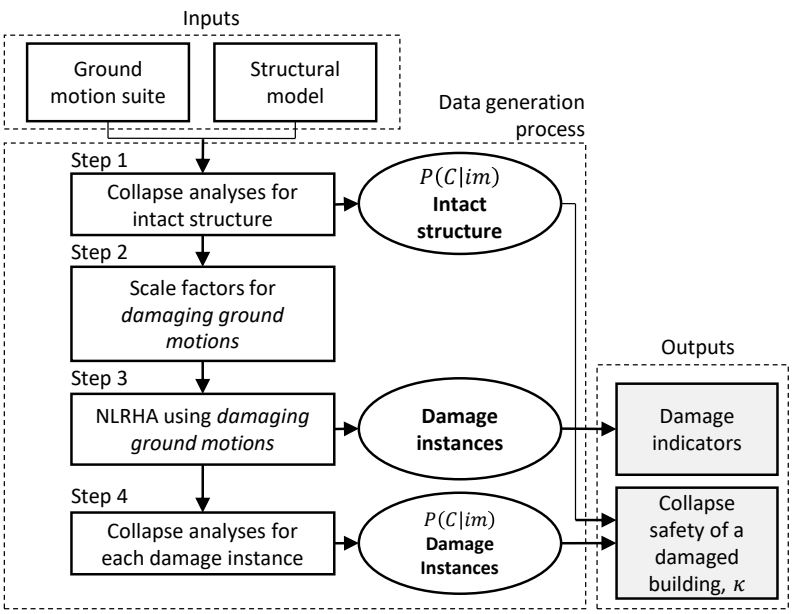

FIGURE 1 Flowchart of safety evaluation of intact and earthquake-damaged structural system.

Given the structural model and input ground motions, the assessment is organized into four main steps. The first step is to perform a collapse analysis of the intact structure to compute its collapse fragility curve ($P[C|im]$), which relates the probability of collapse to the ground motion intensity. This is accomplished using an incremental dynamic analysis (IDA)[20] to compute the ground motion intensity that causes collapse ($IM_{collapse}$) of the intact structure for each of the input ground motions. In IDA, a model of the structure is subjected to successive NLRHAs by scaling each ground motion to the lowest intensity that causes collapse. The resulting data is fit to a cumulative log-normal distribution that describes the structural collapse fragility. This follows the concept of FEMA P695[21] to evaluate collapse safety, although, as described later, the procedure is slightly modified. Figure 2(b) presents example IDA results that are used to compute the intact collapse fragility curve shown in grey in Figure 2(e).

The second step determines the scale factors to obtain "damaging ground motions", which are strong enough to produce damage but not collapse the structure. Figure 2(b) shows the IDA curve of an example ground motion (GM15, in black) and marks four intensities that were used to generate damage. The selected intensities correspond to fractions of the collapse intensity of each separate ground motion. As illustrated in 2(c), these motions produce damage that spans from light to severe.

The third step entails performing the NLRHA of the model using the damaging ground motions to obtain several "damage instances". In this context, a damage instance refers to a unique realization of damage distributed throughout the structure, which can be characterized by scalar damage indicators. As illustrated in 2(c), these motions produce damage that spans from light to severe.

The final step of the process is to perform collapse analyses of each damage instance of the structure to compute the reduced collapse fragility curve. To do this, each of the original ground motions (from Step 1) is concatenated to the damaging ground motion as depicted above Figure 2(d). The analysis is repeated several times, with the second ground motion incrementally amplified until the damaged structure collapses. Conceptually, this analysis sequentially inflicts structural damage with the first ground motion and then assesses the post-earthquake collapse safety by performing a full IDA with the second ground motion. Figure 2(d) shows the IDA curves for each of the damage instances associated with GM15 in Figure 2(c). Note that the IDA curves for each damage instance start from the maximum residual drift caused by the damaging ground motion. The collapse intensities for each ground motion are used to estimate collapse fragility curves for each damage instance (Figure 2(e)). The collapse fragilities shown in Figure 2(e) are further synthesized into a single metric, called the collapse safety ratio, κ, that relates the relative median collapse safety index of a damaged structure to its value when the structure was intact (see Section 2.2 for more detail).

2.1 | Damage indicators

A damage indicator is a scalar measure that represents the post-earthquake damage of a structure.[11] Candidate damage indicators should be selected based on the expected behavior of the structure of interest and could be any scalar quantity that correlates with damage. In general, damage indicators belong to three classes: (1) intensity measures (IM), (2) engineering demand parameters (EDP), and (3) fractions of damaged components. The most common IM-based damage indicator is peak ground acceleration, which is used in the ATC-20 methodology to decide whether inspectors should be deployed after an earthquake. The residual story drift ratio ($SDR_{residual}$)[19] and the peak transient story drift ratio (SDR_{peak})[22] are typical EDP-based damage indicators. $SDR_{residual}$ can be directly measured after an earthquake, while the SDR_{peak} either requires structural instrumentation for a direct measure or an analytical approximation.

The third class of damage indicators, fractions of damaged components (e.g. fraction of beams with cover spalling damage), require an estimate of each component's damage state (DS) for a given damage instance. In a field application, the component damage states can be observed by an inspector. In our simulations, we use the virtual inspector concept[23,24] to estimate the damage state of each component. The virtual inspector employs the Performance-Based Earthquake Engineering framework[25] with analytical component fragility curves to relate EDPs with observable damage states. Component fragility curves give the probability of each damage state, given an EDP. Depending the on the structure, these fragility curves may be readily available, such as the FEMA P58[26] fragility database for most components associated with buildings. For a given component i, the virtual inspector uses the corresponding EDP, estimated from NLRHA of the structure, to compute the probability that the component reaches each possible damage state. The expected damage state of component i (d_i) can be computed as the weighted sum of the discrete damage states using the probabilities of each damage state as the weights.[27] Note that the estimated damage state is a real number between 0 and m (where m = the number of discrete damage states) instead of an integer. The process is repeated for every component in the structure to calculate its expected damage state.

2.2 | Collapse safety of a damaged structure: κ

Collapse safety is tracked using a scalar metric, called κ, which is a ratio between the median values of the collapse fragility curves of the damaged and intact structure. To help account for the influence of spectral shape on collapse behavior[28], the collapse fragility is calculated using average spectral acceleration $Sa_{avg}(T)$[29] as the IM, as calculated following Equation 1:

$$\ln Sa_{avg}(T) = \frac{1}{q}\sum_{i=1}^{q} \ln Sa(T_i); \text{ where } 0.2T \leq T_i \leq 3.0T \tag{1}$$

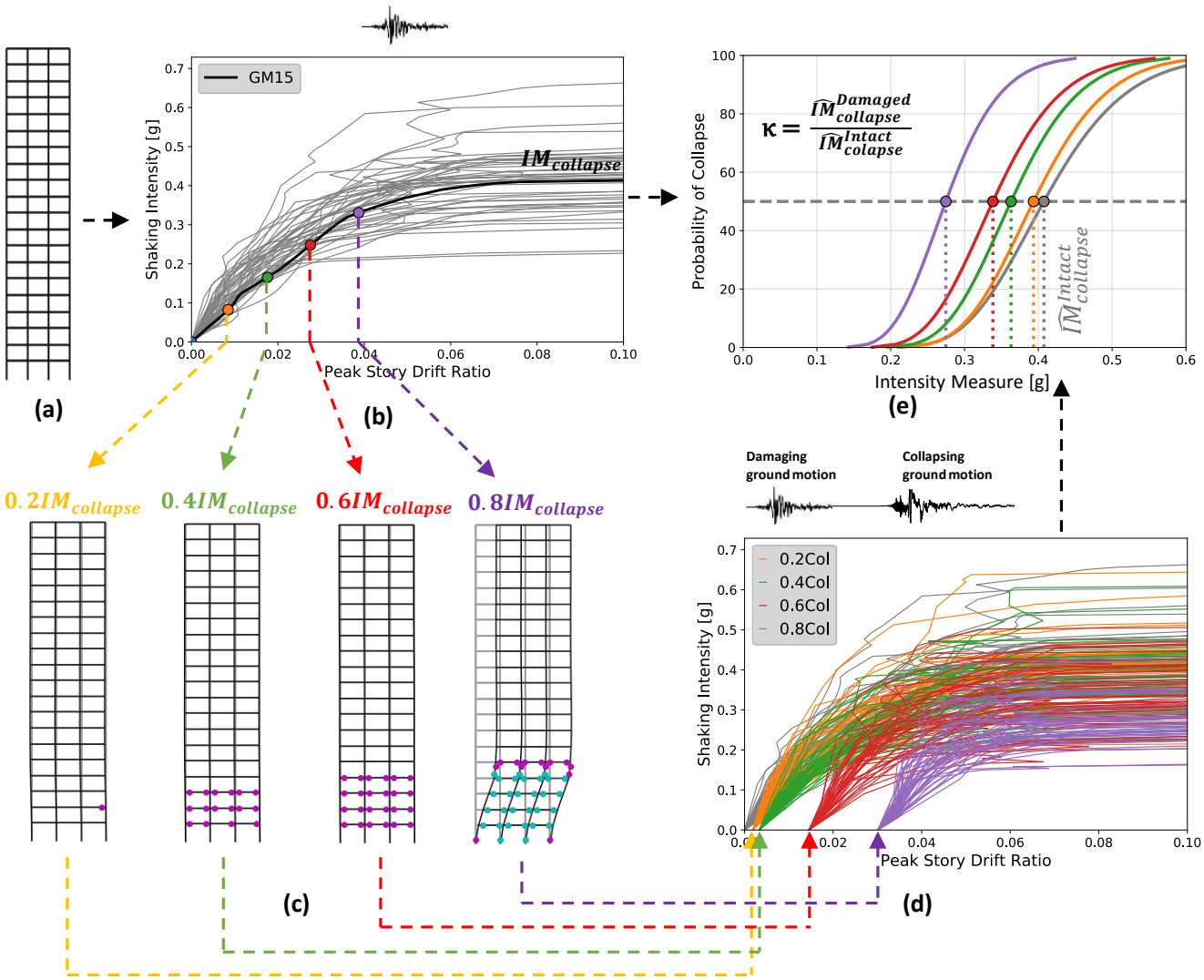

FIGURE 2 Illustrative results of the structural damage and post-earthquake data generation process for a 20-story RC frame building: **(a)** Schematic view of the idealized frame; **(b)** IDA curves for the intact building highlighting four intensities for one ground motion (GM15), prior to collapse; **(c)** Example damage instances of the frame when subjected to the highlighted intensities of ground motion 15 (GM15); **(d)** IDA curves for the frame after reaching each of the damage instances shown in **(c)**; and **(e)** Collapse fragility curve of the intact frame and four damage instances.

The term "average" refers to the geometric mean, or the log-average, taken over q periods within the range between $0.2T$ and $3.0T$, where T is the fundamental (first mode) vibration period of the structure. The periods are linearly spaced at every 0.01 seconds, and the spectral accelerations are 5% damped. By implicitly capturing the spectral shape in the ground motion selection, the target IM of $Sa_{avg}(T)$ avoids the need to apply a spectral shape adjustment to the resulting fragility curves for the unique site hazard, provided that the hazard is characterized by $Sa_{avg}(T)$. In this study, we inferred $Sa_{avg}(T)$ by considering site-specific correlations in the standard $Sa(T)$ intensity measure, similar to approaches used by other research groups.[30,31,32]

The collapse index κ is calculated as the ratio of the median value of the collapse intensity of the damaged, $\widehat{Sa}^{Damaged}_{collapse}$, and intact structure, $\widehat{Sa}^{Intact}_{collapse}$, computed per Equation 2 following Ryu et al.[33] and shown in Figure 2(e). As illustrated in the figure,

κ reflects the leftward shift in the collapse fragility caused by damage, implying that the damage does not significantly affect the dispersion in the fragility curves.

$$\kappa = \frac{\widehat{Sa}_{avg}(T)^{Damaged}_{collapse}}{\widehat{Sa}_{avg}(T)^{Intact}_{collapse}} \tag{2}$$

Worth highlighting is that κ is a relative measure of collapse risk, where the question of post-earthquake reoccupancy of a building presumes that the stakeholders (i.e., building occupants or code officials) consciously or unconsciously accept the risk of using a building in its pre-earthquake condition regardless of what that risk may be compared to some standard or building code. Alternatively, the analyst could redefine κ using a baseline that reflects a code-confirming design by changing the denominator in Equation 2. The data generation process in Figure 1 produces a collection of damage instances of the structure of interest that can be characterized by a set of candidate damage indicators, which are related to the post-earthquake collapse safety index κ.

3 | METHODOLOGY FOR SELECTING DAMAGE INDICATORS AND SAFETY THRESHOLDS

The next step in the safety assessment process is identifying damage indicators that correlate well with κ and quantitative thresholds to inform post-earthquake inspections. The methodology has five steps, plus an optional sixth, as illustrated in Figure 3. The methodology starts from the two main outputs of the data generation process described in Section 2: damage indicators for each damage instance and corresponding values of the collapse safety ratio, κ. The first step, described in Section 3.1, relates the calculated collapse safety ratio κ to each damage indicator by fitting a trilinear model to the data. The fitted trilinear models suggest tagging thresholds for each damage indicator and a limiting value of the collapse safety ratio, κ_{limit}, at which the safety of the damaged structure starts to degrade rapidly. In the second step, the mean absolute error of the trilinear models is used to evaluate the efficiency of the damage indicators to estimate κ and discard the least efficient damage indicators (Section 3.2). The third step selects optimal tagging threshold values for the remaining candidate damage indicators, where the optimal threshold is chosen to maximize the correctness of tagging decisions (i.e., by minimizing false green and red tags), measured by a metric called "tagging accuracy" that is based on concepts of statistical classification algorithms. In step 4, the robustness of each threshold and damage indicator is assessed with respect to modeling uncertainty using the sensitivity analysis described in Section 3.4. Finally, in Step 5, the most promising damage indicators and thresholds are evaluated to determine thresholds that can be applied in post-earthquake field evaluations (Section 3.5). As an optional sixth step, the trilinear model of the selected damage indicators can be used to compute collapse fragility curves conditioned on the value of the damage indicator, as explained in Section 3.6.

3.1 | Step 1: Conditioning collapse safety on a damage indicator

Referring to Figure 4(a), a trilinear model is proposed to identify the damage indicators that are good predictors of κ and reveal thresholds that help inform safety decisions. The model is a descending function, fitted to κ with respect to the logarithm of the damage indicators, following Eq.3). The trilinear shape is informed by the data, as will become apparent in subsequent figures for the case study.

$$\tilde{\kappa} = \begin{cases} \kappa_0 & \text{if } DI < a_1 \\ \kappa_0 + b_1(\ln(DI) - \ln(a_1)) & \text{if } a_1 \leq DI < a_2 \\ \kappa_0 + b_1(\ln(a_2) - \ln(a_1)) + b_2(\ln(DI) - \ln(a_2)) & \text{otherwise} \end{cases} \tag{3}$$

A descending function was selected because an increase in damage (i.e., a larger value of damage indicator) reduces κ, and the trilinear function has the potential to uncover two kink values that may be useful thresholds for safety decisions. The models start with $\kappa = \kappa_0$ at a predefined minimum value of the damage indicator, DI_{min}, which was chosen to avoid singularities when working in log space. The model has five parameters: the initial κ_0, first kink value (a_1), initial slope (b_1), second kink value (a_2), and secondary slope (b_2). a_1 indicates the maximum amount of damage for which the performance reduction is negligible. a_2, labeled "cliff threshold" in Figure 4(a), reveals the amount of damage at which the collapse safety of the damaged

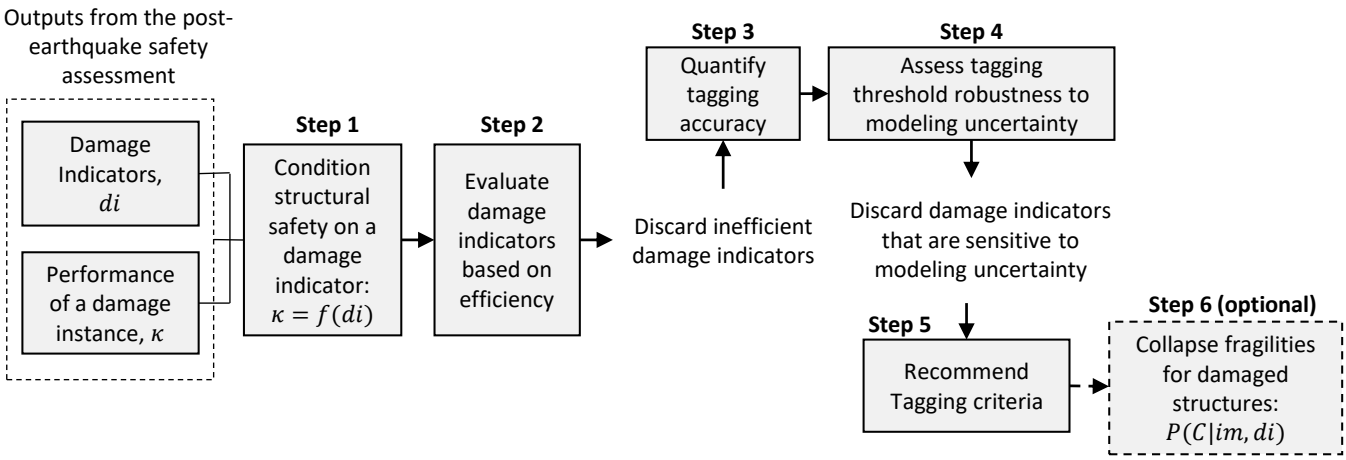

FIGURE 3 Summary of the process to compare and select appropriate damage indicators and tagging thresholds for post-earthquake safety evaluations. The process can be extended with a sixth step to obtain collapse fragilities conditioned on damage indicator values.

structure starts degrading at a dangerous rate. The function fitting process minimizes the sum of the squared error using practical recommendations by Magnani and Boyd[34] to find the best local minimum for Equation 4 with the following constraints.

$$\min \sum_{i=1}^{n} (\kappa_i - \hat{\kappa})^2 \tag{4}$$

$$a_1 \leq a_2 \tag{5}$$

$$0.9 \leq \kappa_0 \leq 1.1 \tag{6}$$

where n is the total number of [κ, damage indicator] pairs in the data. The ratio κ is allowed to take values up to 1.10 to account for the few damage instances where the median collapse capacity is slightly larger than for the intact structure (reasons for values above 1.0 are explored later in the case study). This trilinear model can be used to directly estimate the collapse fragility of a damaged structure by conditioning the median collapse intensity on a damage indicator value as shown for the dots in Figure 4(a) and the corresponding fragilities in Figure 4(b).

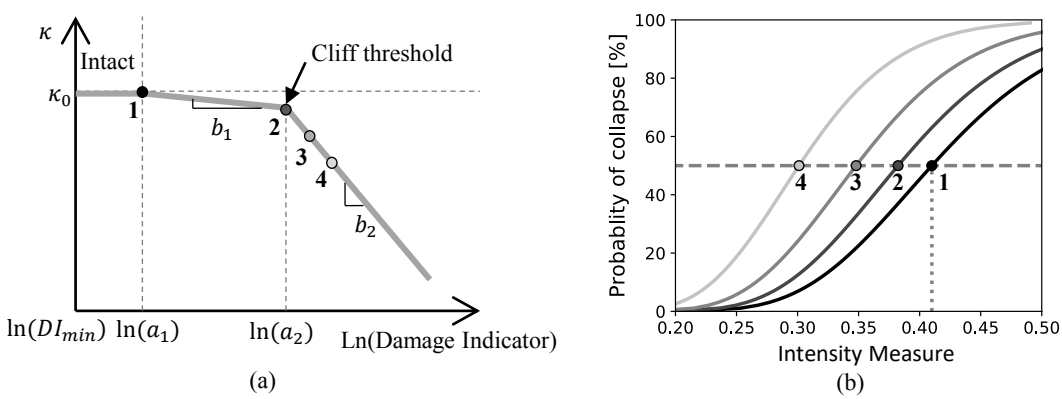

FIGURE 4 Relationship between damage indicator and collapse safety **(a)** Tri-linear model to estimate the κ as a function of a damage indicator; and **(b)** Collapse fragilities conditioned on the damage indicator value.

While more elaborate models have been proposed in other studies to estimate κ as a function of several damage indicators for specific structures[13], they are difficult to extend to various structural systems. We have opted for a simpler model to identify key trends more suitable for practical implementation in the field.

3.2 | Step 2: Evaluate damage indicators based on efficiency

The ability of each damage indicator to estimate κ is quantified in terms of "efficiency", defined in this context as the capacity of a damage indicator to explain most of the variability in κ, similar to how efficiency has been defined in the evaluation of intensity measures.[35] Efficiency can be measured by estimating the mean absolute error (*MAE*) of each damage indicator based on the corresponding trilinear model as shown in Equation 7, where n is the total number of [κ, damage indicator] pairs in the data. *MAE* is preferred over other alternatives (e.g. mean squared error) because the error measure is in the same units of κ. More efficient damage indicators have lower MAE; thus, this metric allows us to rank the damage indicators and eliminate from consideration the least efficient ones.

$$MAE = \frac{\sum_{i=1}^{n} |\kappa_i - \hat{\kappa}|}{n} \tag{7}$$

3.3 | Step 3: Quantify Tagging Accuracy

Any safety recommendation will have an imperfect accuracy, resulting in false red tags (safe structures deemed unsafe) and false green tags (unsafe structures deemed safe). This step of the methodology presents a metric to quantify the accuracy of safety criteria and, thereby, determine a threshold value that maximizes tagging accuracy for each damage indicator.

A useful damage indicator allows the identification of those damaged structures that are unsafe (i.e., have a low value of κ). The question is, what is the κ_{limit} value to differentiate between safe and unsafe damaged structures? Previous researchers typically chose κ_{limit}=0.9 without much explanation and highlighted that this limit should be ultimately chosen by the stakeholders since it reflects their risk perception.[33,12,13]

To inform the selection of the threshold, we employ the concept of balanced accuracy, which is common for comparing binary classifiers in statistical modeling.[36] The balanced accuracy, renamed tagging accuracy in this context, is the average fraction of correct green tags and the fraction of correct red tags as shown in Equation 8.

$$\text{Tagging accuracy} = \frac{1}{2}\left(\frac{CG}{TG} + \frac{CR}{TR}\right) \tag{8}$$

where: CG = Correct green tags (Damage instances with Damage Indicator $\leq$ Threshold)
TG = True green tags (Damage instances with $\kappa > \kappa_{limit}$)
CR = Correct red tags (Damage instances with Damage Indicator > Threshold)
TR = True red tags (Damage instances with $\kappa \leq \kappa_{limit}$)

The computation of tagging accuracy requires prior knowledge of an accurate safety measure of each damage instance. We assume a safety measure defined by a κ_{limit}, such that any damage instance with $\kappa \leq \kappa_{limit}$ is a reliable red tag. The κ_{limit} is not an arbitrary choice; rather, it is informed by the cliff thresholds from multiple damage indicators, where the tagging accuracy puts equal weights on false red and green tags. This definition could be modified to give more weight to false green tags, but we chose to use a balanced metric so that the cliff thresholds provide an unbiased measure. In this approach, the risk perception of the stakeholders can be incorporated into the safety assessment by changing the κ_{limit} from that suggested by calculated thresholds. Note that the lowest possible tagging accuracy is 0.50, which occurs for two trivial thresholds: (1) zero threshold, so all damage instances are red-tagged, or (2) a very large threshold, so all damage instances are green-tagged.

In actual post-earthquake inspections, safety tags are determined only by the observed damage indicator values, i.e., without the knowledge of detailed structural analyses. Thus, the optimal safety threshold for any damage indicator should maximize the tagging accuracy. We use a grid search algorithm to find the threshold value of each damage indicator that maximizes tagging accuracy. The grid search for each damage indicator can be implemented in the following sequence of steps: (1) identify the lowest and highest values of the damage indicator; (2) set the lowest value as the safety threshold; (3) assign red tags to all damage instances with damage indicators larger than the threshold and green tags otherwise; (4) compute the tagging accuracy using the true tags based on the selected κ_{limit} of the structure; and (5) increase the threshold value and repeat steps 3 and 4 until

reaching the highest value of the damage indicator. The threshold value with the maximum tagging accuracy is optimal. The next step in the methodology is to evaluate the damage indicators based on their robustness to modeling uncertainty.

3.4 | Step 4: Assess the safety threshold robustness to modeling uncertainty

In most post-earthquake inspections, the quality of construction and the properties of the structural materials are not precisely known, which leads to uncertainties in modeling the structural response. The modeling uncertainty affects the threshold values discussed in the previous step of the methodology. Ideally, an appropriate damage indicator would provide a safety threshold value relatively insensitive to the structural modeling uncertainty.

To compare the robustness of various damage indicators to modeling uncertainty, we use a sensitivity study to identify model parameters that have the largest influence on the structural response. We then set realistic upper and lower bounds for each parameter (typically one standard deviation above and below their mean values). Using these bounds, we generate a low- and high-quality version of the structural model.

The data generation process described in Section 2 is repeated for the low- and high-quality versions of the structural model. The trilinear model is fitted to the resulting data to observe the effect of model uncertainty on the critical threshold. While further investigation could include randomization of the parameters, the simpler sensitivity approach quickly identifies whether the damage indicator is affected by the uncertainty. A damage indicator is considered robust to modeling uncertainty if the resulting trilinear models for each model realization (low- mean- and high-quality) are similar. As with efficiency, the robustness evaluation allows comparisons of damage indicators, and the indicators overly sensitive to changes in the model parameters are dropped from further consideration.

3.5 | Step 5: Recommend safety criteria for the structure

Recommendations for post-earthquake evaluations for a particular structure can be based on the thresholds of efficient and robust damage indicators identified from steps 1 to 4 of this methodology. This process may be especially useful to develop tailor-made inspection criteria for special and complex structures, such as tall buildings and public buildings with large occupancy, but it is also useful to develop recommendations for broader structure types (e.g. regular ductile RC buildings, wood frame houses). In the latter context, the final recommendation requires a general threshold that balances results from a group of representative archetypes for the structural type.

3.6 | Step 6 (Optional): Collapse fragilities for damaged structures

The post-earthquake assessment presented here focuses on a relative measure of the increase in vulnerability of a structure due to earthquake damage. As such, this assessment does not consider the absolute value of risk or the influence of elevated earthquake aftershock hazard on the risk. For decision-making regarding reoccupancy of buildings following a major earthquake, one may want to consider the increased collapse risk due to structural damage and aftershock hazard. Such an analysis would require the collapse fragility curve of the structure for its condition following a mainshock earthquake. The trilinear model presented in Figure 4(a) provides a straightforward method to determine the collapse fragility of the structure Figure 4(b) under various amounts of damage, based on the damage indicator. The inputs for this process are the fitted trilinear model for κ as a function of a selected damage indicator, the intact collapse fragility curve, and the damage indicator value determined by post-earthquake inspection. In addition, one would need information to characterize the site-specific hazard considering both the steady-state earthquake hazard and the elevated earthquake hazard. Details of such an approach are described in a related paper by the authors[37].

4 | APPLICATION OF THE METHODOLOGY TO DUCTILE RC FRAME BUILDINGS

This section illustrates the proposed methodology with a case study of ductile RC frame buildings. We start by describing the ground motion suite and the detailed models used for generating structural damage and post-earthquake data, as well as the candidate damage indicators relevant to ductile RC frames. Then, we proceed through each step of the proposed methodology. Ultimately, we find that the best-performing damage indicator is one that combines beam and column hinge damage indices

on a floor-by-floor basis and combines them to produce a building index. Key attributes of this indicator are that it: (1) is least sensitive to modeling uncertainty; (2) is the most efficient in predicting collapse safety; and (3) has safety thresholds that are consistent across building models with varying numbers of stories.

4.1 | Inputs for structural damage and post-earthquake data generation

Following the procedures outlined in Section 2, the data generation process requires input ground motions and models that represent the structures of interest. This section describes our choices for the case study.

4.1.1 | Ground Motions

Similar to Burton and Deierlein,[15], this case study uses the FEMA P695 far-field ground motion suite (Figure 5a) for both the damaging and collapsing earthquakes. The two horizontal components of the 22 ground motion pairs of the suite were considered independently, for a total of 44 records.

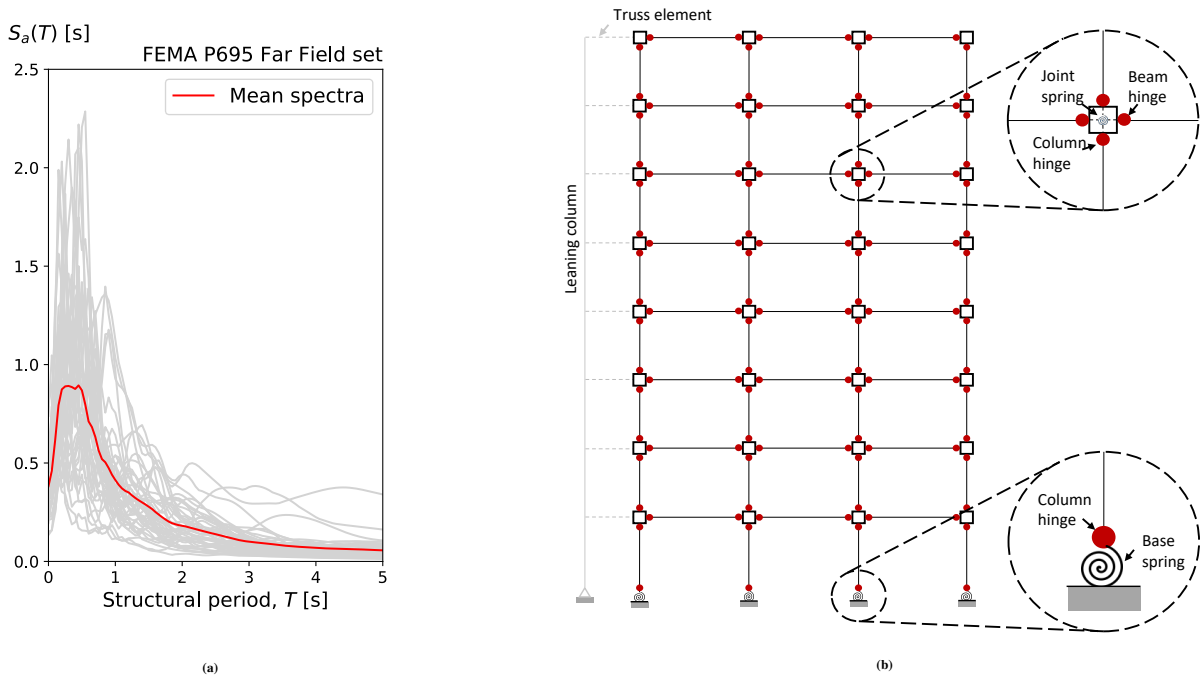

FIGURE 5 Input ground motions and structural model for the case studies **(a)** Ground motion spectra for FEMA-P695 far field set. **(b)** Idealized analysis model of the ductile RC frame buildings.

4.1.2 | Building Models

The ductile RC frame buildings are described by four archetypes per the ASCE-7[38] and the ACI-318[39] specifications for a high seismic hazard location in Los Angeles on soil class D. The archetype designs and numerical models were developed previously by Haselton et al.[40]. Table 1 shows the number of stories, the fundamental period of vibration, the design-based earthquake (DBE) $Sa(T)$, and the archetype identifier for each model. The archetypes were idealized as two-dimensional frames and modeled using OpenSees.[41] Figure 5b illustrates the main features of the analytical models for each frame, where beam and column hinges are lumped plasticity elements using the IMK model[42], specifically calibrated for RC elements.[43] The flexibility of beam-column joints is represented by an elastic spring implemented by the Joint2D[44] element in OpenSees. The column bases have elastic rotational springs to represent foundation flexibility. The destabilizing effects of the gravity framing are included by means of a leaning column. We used the hinge model parameters, developed by Haselton et al.[43] and enhanced by Gokkaya

et al.[18], to determine the low-and high-quality version of each archetype building model. The concentrated plastic hinges that simulate the non-linear responses of the concrete members are uniaxial springs, which do not explicitly model axial-flexure interaction. The hinge parameters are set based on the column gravity forces, assuming that the variation in axial loads under earthquakes has a negligible effect on the collapse of the ductile RC frames (supported by Harrington and Liel[45]).

TABLE 1 Attributes of the RC-frame structures considered.

Number of stories	Fundamental period* [s]	$Sa(T)^{DBE}$ [g]	Archetype identifier
4	0.95	0.63	1008
8	1.80	0.33	1012
12	2.14	0.27	1014
20	2.35	0.25	1021

*The initial stiffness uses cracked section properties calibrated by Haselton et al.[43]

The data-generation process for each RC frame uses 44 records at seven intensities for the damaging earthquakes, for a total of 308 damage instances described by the candidate indicators introduced in Section 4.1.3. For each damage instance, collapse assessments were subsequently carried out with full IDA, using each of the 44 ground motions as a collapsing earthquake. In total, approximately 250,000 NLRHA were performed for each archetype and each model quality version. This large computational task was completed by running the OpenSees parallel computing interpreter (OpenSeesMP) with high-performance computing resources. The entire data set generated is available for download (see Section 6) to enable further studies without the need to spend large computational resources again.

4.1.3 | Candidate damage indicators

The candidate damage indicators for ductile RC-frame buildings are summarized in Table 2. The $SDR_{residual}$ and SDR_{peak} indicators are depicted in Figure 6 for an example response of the 8-story archetype. Note that calculations of the transient SDR_{peak} and $Sa(T)$ in an actual post-earthquake scenario would require instrumentation that is not generally available. However, information on nearby stations can be used to obtain acceptable estimates of the $Sa(T_1)$ using spatial correlation models, while SDR_{peak} can be estimated using simplified building models.

TABLE 2 Description of candidate damage indicators.

Damage Indicator ID	Damage indicator description
SDR_{peak}	Maximum story drift ratio
$SDR_{residual}$	Maximum residual drift ratio
FDI_{max}	Maximum floor damage index
FDI_{max}^{bottom}	Maximum floor damage index of the bottom $N_{mechanism}$ floors; $N_{mechanism}$ is 1, 2, 3 and 5 for a 4-, 8-, 12- and 20-story building, respectively (counting floors above the ground level)
Beams DS≥1	Fraction of beams at any damage state

The floor damage indices, FDI_{max} and FDI_{max}^{bottom}, are inspired by FEMA-352's[5] damage index for pre-Northridge steel moment frames. According to FEMA-352, a damage state from 0 to 4 is assigned to each beam-column connection on each floor, based on the observed damage. The damage state of each component (d_i for the i-th component) is used to compute a floor damage index (FDI) from 0 to 1, where 1 means that all beam-column connections are fractured. Applying this idea to ductile RC-frames, the beam and column hinge damage indices on each floor are combined to compute FDI using Equation 9.

$$FDI_i = \frac{0.5}{n_b}\sum_{j=1}^{n_b}\frac{d_{bj}}{3} + \frac{0.5}{n_c}\sum_{j=1}^{n_c}\frac{d_{cj}}{3} \tag{9}$$

where: n_b = Number of beam moment connections in floor i,
n_c = Number of column moment connections adjoined to floor i,
d_{bj} = Damage state of beam j (3 damage states per component), and
d_{cj} = Damage state of column j (3 damage states per component).

Note that the damage state of each component in Equation 9 is divided by 3, the total number of damage states in this case. Figure 6 shows an example of the damage state of each beam and column hinge and the corresponding computation of FDI in the fourth floor and the 8-story frame archetype. Candidate damage indicators can be crafted by combining the FDI's over the height of the building. Based on a review of potential FDI combinations, we propose FDI_{max} and FDI_{max}^{bottom}. The latter is more practical than the former because it only requires information about the bottom quarter of the building (see $N_{mechanism}$ in Table 2) to take advantage of the fact that the most common collapse mechanisms of RC frames engage stories in that part of the structure.[46] Table 3 summarizes the component fragilities used in the virtual inspector to estimate the damage state of each component (d_i).

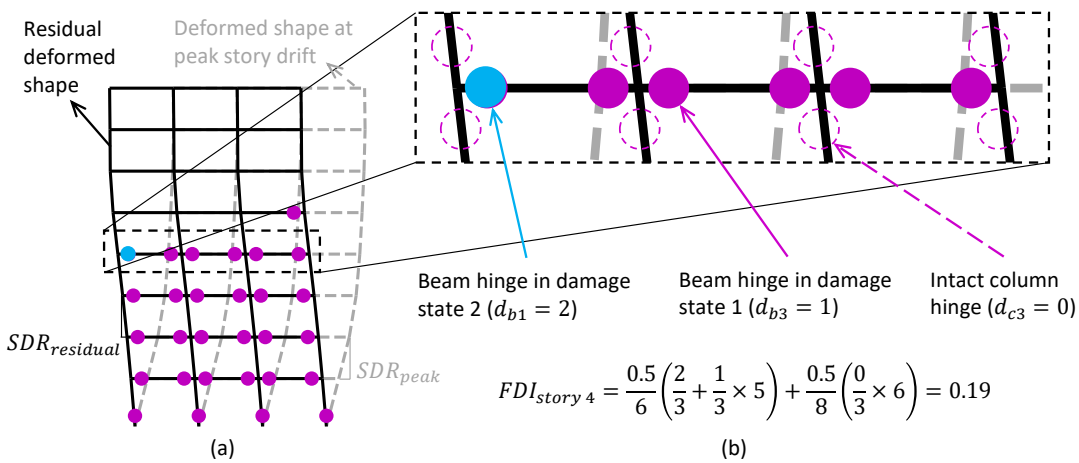

FIGURE 6 Identification of various damage indicators used to characterize the post-earthquake performance of RC-frames. **(a)** Elevation of the 8-story archetype after a damaging earthquake showing the residual deformed shape in black, the deformed shape at the transient peak story drift in grey, and the hinges that have formed in colors. **(b)** Closer look at the fourth floor of the building and example computation of the corresponding FDI

4.2 | Condition collapse safety on a damage indicator

Data is assembled for each damage indicator and plotted versus κ, and the trilinear model was fit to the data for each of the four RC frame archetypes. Figure 7 shows the models (the black lines) as a function of selected damage indicators for the 8-story archetype (Figure 7(a)-(c)), 20-story archetype (Figure 7(d)-(f)), and all archetypes combined (Figure 7(g)-(i)). The underlying data is presented as a scatter plot color coded per building. Visual scrutiny of the plots in Figure 7 suggests that the trilinear model is a reasonable representation of the relationship between κ and the candidate damage indicators. Nevertheless, the dispersion of the points around the black line varies for each damage indicator, suggesting that their ability to estimate κ is different. The first kink, a_1, is the value up to which the collapse safety of the building is not expected to vary from the intact, as stated in Section 3.1. This kink may provide useful information as is the case of SDR_{peak}, where a_1 suggests that peak drifts lower than 1.0% and 0.7% do not affect the collapse safety of the 8-story and 20-story archetype, respectively.

The second kink, a_2, is the cliff threshold. In all plots of Figure 7, this value marks a sudden change in the rate a which κ decreases, suggesting that it is a reasonable threshold for differentiating between collapse performance. The cliff threshold for SDR_{peak} is around 2.3-2.5% for all buildings, which is in accordance with the drift limits in modern design codes. Similarly, the cliff threshold for FDI_{max} is 0.15-0.17. This value corresponds to the FDI for a floor with all beam hinges at DS1., as defined

TABLE 3 Component fragility for observable damage of beam and column hinges (adapted from Burton et al.[12] based on FEMA P-58[26]).

Component	Damage State	Damage description	Median EDP	Dispersion
Beam hinge	DS1	Numerous residual cracks (width > 0.06in) extended one section depth from element end	$0.30\theta_c$	0.40
	DS2	Concrete spalling	$0.70\theta_c$	0.40
	DS3	Concrete core crushing, longitudinal rebar buckling or fracture	$1.00\theta_c$	0.40
Column hinge	DS1	Numerous residual cracks (width > 0.06in) extended one section depth from element end	$0.25\theta_c$	0.40
	DS2	Concrete spalling	$0.55\theta_c$	0.40
	DS3	Concrete core crushing, longitudinal rebar buckling or fracture	$0.80\theta_c$	0.40

θ_c: Capping rotation of the IMK hinge model

in Table 3. The cliff threshold for Beams DS ≥ 1 is noticeably less stable across archetypes compared to the other two damage indicators. This concern is discussed in the next step.

4.3 | Evaluate damage indicators based on efficiency

Figure 8 shows the MAE for all the damage indicators (left to right) and each building archetype (colored lines). The black line in Figure 8 presents the MAE computed for the data of all the archetypes combined (see scatter plots from Figure 7(g)-(i)). This combined MAE is a good metric to evaluate the efficiency of each damage indicator for a broad range of RC frames, rather than the individual archetypes. From Figure 8 it is evident that FDI_{max} and FDI_{max}^{bottom} are consistently the most efficient, followed by the drift indicators (SDR_{peak} and $SDR_{residual}$). The Beams DS ≥ 1 and $Sa(T)/Sa(T)^{DBE}$ damage indicators are the least efficient options. Figure 8 reveals that the MAE for the combined data does not always lay in the center of the lines for individual archetypes. This is particularly evident for the Beams DS ≥ 1 indicator. This occurs because the fraction of damaged beams necessary to reach a given κ changes with the number of stories, which is reflected by the clustering of data points of the same color in Figure 7(i). This means that for taller archetypes, lower damage fractions cause the same reduction in collapse safety compared to shorter archetypes. Combining these disparate responses in a single trilinear model across all the archetypes decreases the efficiency as compared to any one archetype's model.

The lower efficiency of Beams DS ≥ 1 and $Sa(T)/Sa(T)^{DBE}$ implies that post-earthquake evaluations based on thresholds in ground motion intensity or fractions of damaged components can be significantly improved if attention is shifted to more relevant damage indicators. Therefore, the Beams DS ≥ 1 and $Sa(T)/Sa(T)^{DBE}$ are not discussed further in subsequent sections of this paper.

4.4 | Threshold selection

To select a damage indicator threshold, we need to select a κ_{limit} value that accurately estimates the simulated red and green tags (Section 3.3), and then measure accuracy in predicting the simulated tags. To inform the selection of κ_{limit}, Figure 9 shows the value of κ at the cliff threshold for the remaining damage indicators and all archetypes. In most cases, κ at the cliff threshold falls between 0.8 and 0.95 regardless of damage indicator and archetype. The only exception is the 4-story building for SDR_{peak} and $SDR_{residual}$, where the cliff-based κ is heavily affected by the noise in the data. The cliff thresholds for FDI_{max} and FDI_{max}^{bottom} are all approximately $\kappa = 0.85$.

Setting κ_{limit} to 0.85, we can apply a grid search algorithm and compute the tagging accuracy for varying values of each damage indicator, as illustrated in Figure 10(a)-(b) for SDR_{peak} and Figure 10(c)-(d) for FDI_{max}. Results are presented for the 20-story archetype only due to space limitations. The scatter plots in Figure 10(a) and (c) have the color of the true tag according to the κ_{limit} selected; thus, all damage instances above 0.85 should be tagged green, or red otherwise. For a given damage indicator threshold, the points in the lower left or upper right quadrant correspond to damage instances that are assigned an

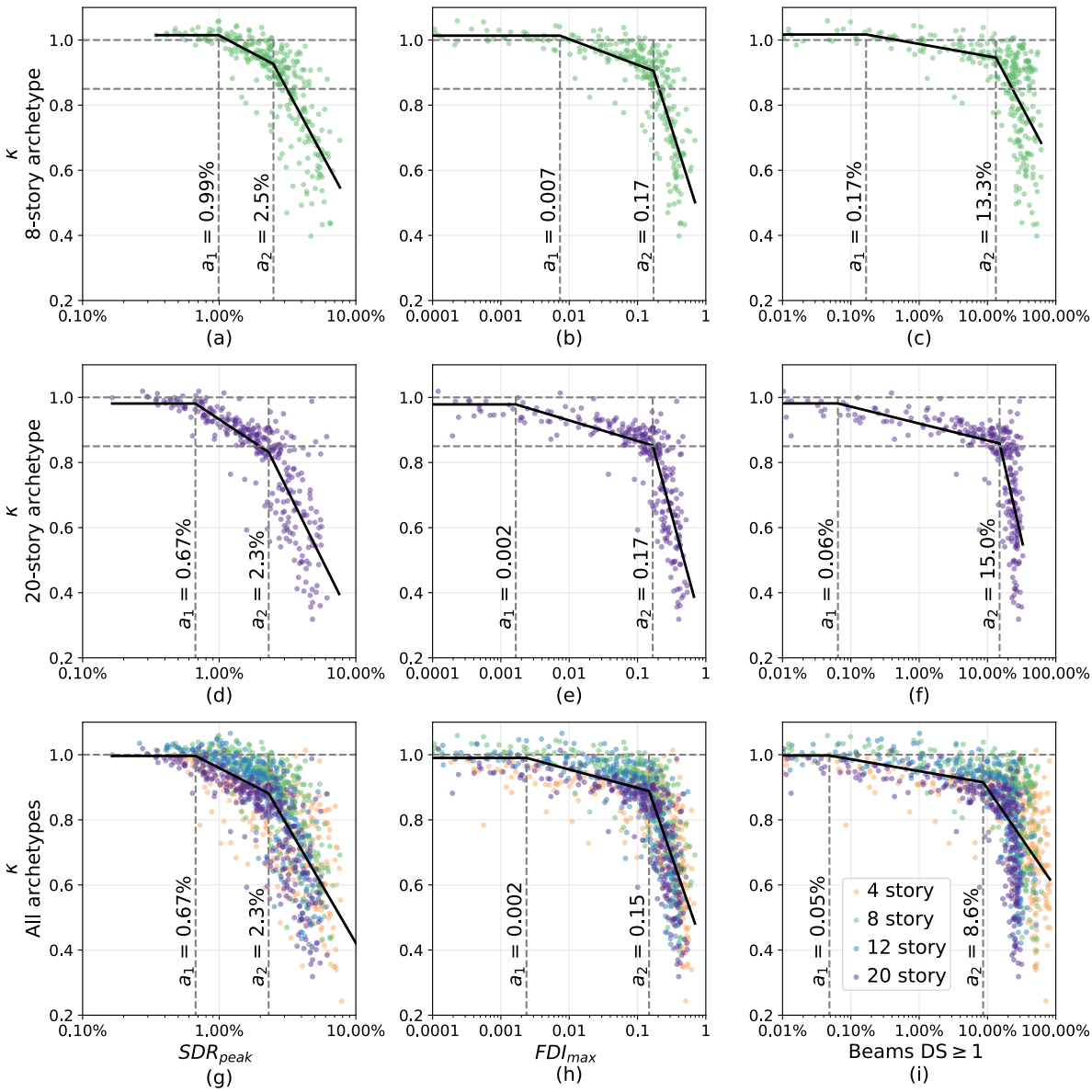

FIGURE 7 Collapse safety ratio κ as a function of selected candidate damage indicators (SDR_{peak}, FDI_{max}, and Beams DS $\geq$ 1) for the 8- and 20-story archetypes, as well as all archetypes combined.

incorrect tag. The plots in Figure 10(b) show the resulting tagging accuracy for a SDR_{peak} threshold ranging from 0.1% to 10% story drift and the plots in Figure 10(d) for a FDI_{max} between 0.01 to 1. The threshold value that maximizes tagging accuracy can be read directly from the plots in 10(b) and (d). SDR_{peak} achieves a maximum accuracy of 87% at a 2.0% threshold, again, in accordance with modern design codes. FDI_{max} has a similar value for maximum accuracy of 0.16. This value agrees with the cliff threshold discussed in Section 4.2.

To inform the choice of a damage indicator-based safety recommendation, Figure 11 shows various options for the safety thresholds for the four candidate damage indicators. The solid grey line marks the cliff threshold for each archetype, while the dot-dashed grey line shows the constant cliff threshold obtained by combining the data for all archetypes together (as depicted in Figure 7(g)-(i)). The purple lines show the optimal threshold for three alternative κ_{limit}: 0.80, 0.85, and 0.90.

In most cases, the cliff thresholds and the maximum accuracy thresholds tend to decrease with the number of stories. However, Figure 11 helps to identify safety thresholds that are general for all archetypes as intended by the combined threshold that

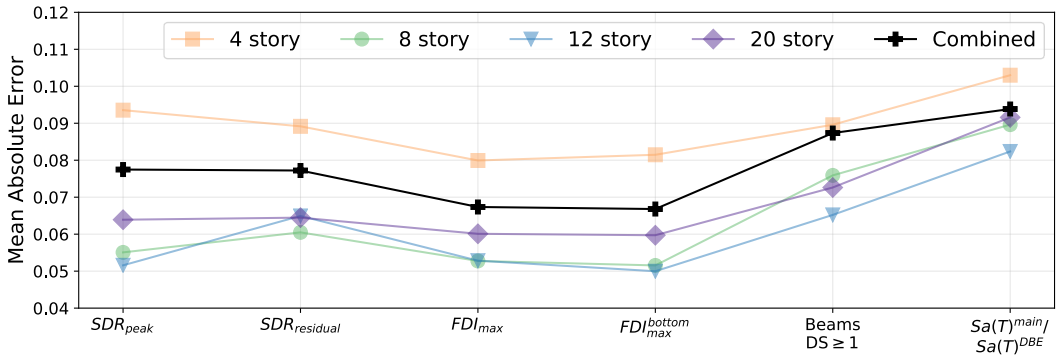

FIGURE 8 Efficiency of candidate damage indicators for the 4-, 8-, 12-, and 20-story RC-frame archetypes. The Beams DS ≥ 1 and $Sa(T)/Sa(T)^{DBE}$ damage indicators have the largest mean absolute error, and, thus, are the least efficient to predict κ. Thus, they will be discarded.

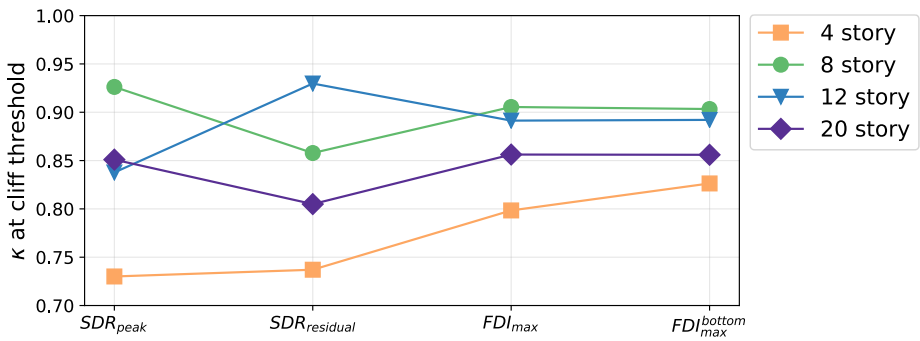

FIGURE 9 Collapse safety ratio κ at the cliff threshold for drift-based damaged indicators, FDI_{max} and FDI_{max}^{bottom} for all RC frame archetypes.

consider the data of all archetypes together. Broadly speaking, for a κ_{limit} of 0.85, the optimal threshold of SDR_{peak} lies between 2.0% and 3.0%. For $SDR_{residual}$ it is between 0.5% and 1.5% and for FDI_{max} and FDI_{max}^{bottom} between 0.14 and 0.20.

Each of the proposed damage indicators can be evaluated based on their maximum accuracy threshold to determine which constitutes the best safety threshold for each building archetype. Figure 12(a) presents the maximum tagging accuracy for each archetype and damage indicator computed using $\kappa_{limit} = 0.85$. These values are the largest possible tagging accuracy that each damage indicator can offer. Note that the drift damage indicators have slightly lower tagging accuracy as compared to the FDI_{max} and FDI_{max}^{bottom} for the shorter archetypes. A similar behavior is observed for a fraction of correctly classified red tags in Figure 12(b). Before deciding on the damage thresholds that are best to represent a broader set of RC buildings, their sensitivity to model uncertainty should be considered.

4.5 | Assess the safety threshold robustness to modeling uncertainty

To evaluate sensitivity to the modeling parameters, we recomputed the backbone of each plastic hinge with parameters set to one standard deviation above and below the median parameters of strength and ductility.[40] The stronger and more ductile backbones are intended to represent a structure with high-quality components, while the weaker and less ductile backbones belong to a structure with low-quality components. Figure 13 presents the pushover curves for uniform lateral loading of the three model versions for the 8-story archetype. Varying the modeling parameters in this way changes the building's lateral strength (maximum base shear on the y-axis) by about 30%. The displacement capacity (roof drift on the x-axis) in the low-quality version is reduced by 30% while the high-quality version's displacement capacity almost doubles with respect to the median model.

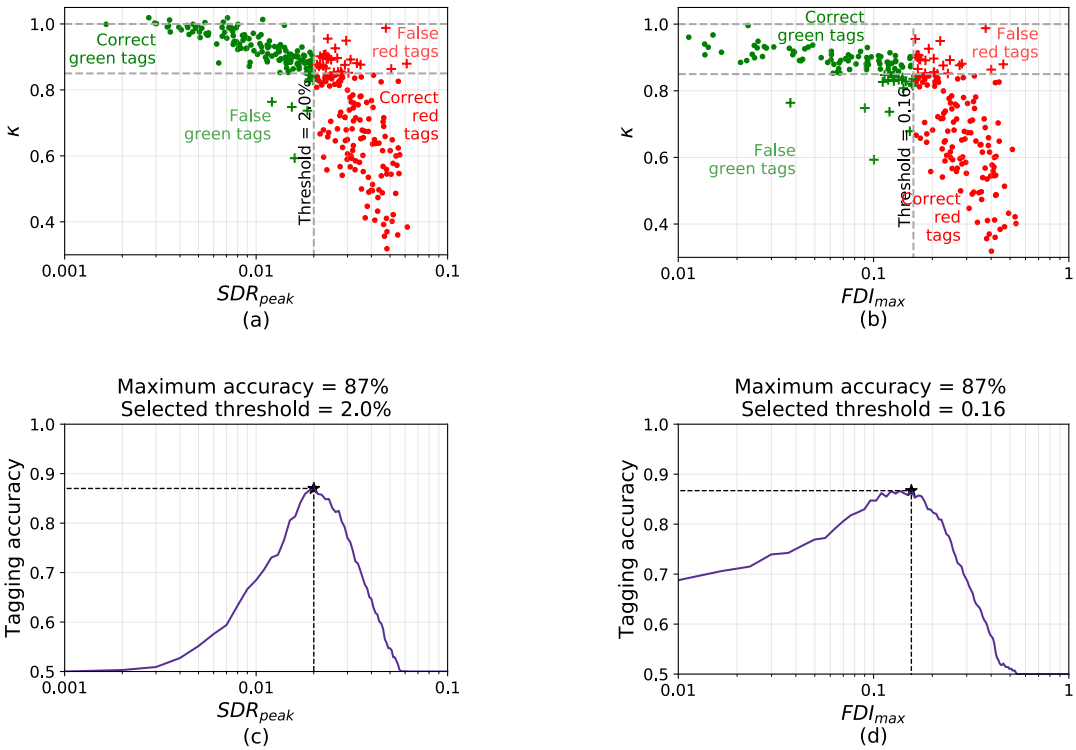

FIGURE 10 Scatter plot of κ as a function of **(a)** SDR_{peak} and **(b)** FDI_{max} including a vertical line at the threshold that maximizes accuracy. The colors show the "true" tags defined by a prescribed $\kappa_{limit} = 0.85$. Cross markers depict miss-tagged damage instances, either false green tags (lower-left quadrant) or false red tags (upper-right quadrant). The tagging accuracy as a function of the damage indicator threshold is shown for **(c)** SDR_{peak} and **(d)** FDI_{max}.

The post-earthquake safety assessment was also carried out for the low and high-quality versions of the 8-story building to observe the effect of the building quality on the threshold values. The resultant trilinear models are presented in Figure 14 for SDR_{peak}, $SDR_{residual}$, FDI_{max}, and FDI_{max}^{bottom}.

The sensitivity analysis demonstrates that drift-based damage indicators are not robust to modeling uncertainty. The trilinear models for SDR_{peak} and $SDR_{residual}$ change significantly with the building quality. The better the quality, the larger the required drift for the same κ value. This is consistent with our intuition for what causes observable damage. A low-quality building has larger displacement demands than the median due to its reduced lateral strength, which promotes premature non-linear excursions. These higher displacement demands affect components that have a low rotational capacity, causing them to deteriorate faster than components in the median model. On the other end, a high-quality building drifts less than the median and suffers less component deterioration, not only due to the limited demand but also to its larger rotation capacity. In addition to the lack of robustness to modeling uncertainty, the safety thresholds for $SDR_{residual}$ are further affected by the lack of accuracy of the concentrated plastic hinge models in terms of estimating residual displacements, which places an additional disadvantage to this candidate damage indicator. In contrast, the trilinear models for FDI_{max} and FDI_{max}^{bottom} are less affected by building quality and are reasonably well predicted by the simulation models. These results reveal that drift-based damage indicators, which are the focus of numerous studies [11,10,47], are in fact more sensitive to modeling uncertainty compared to other damage indicators, which may cause inaccurate safety decisions.

Conversely, FDI_{max} and FDI_{max}^{bottom} implicitly capture modeling uncertainty because they measure damage directly; therefore, a high-quality building that has fewer displacement demands and large component capacities would naturally have less damage, which would be reflected in low FDI values.

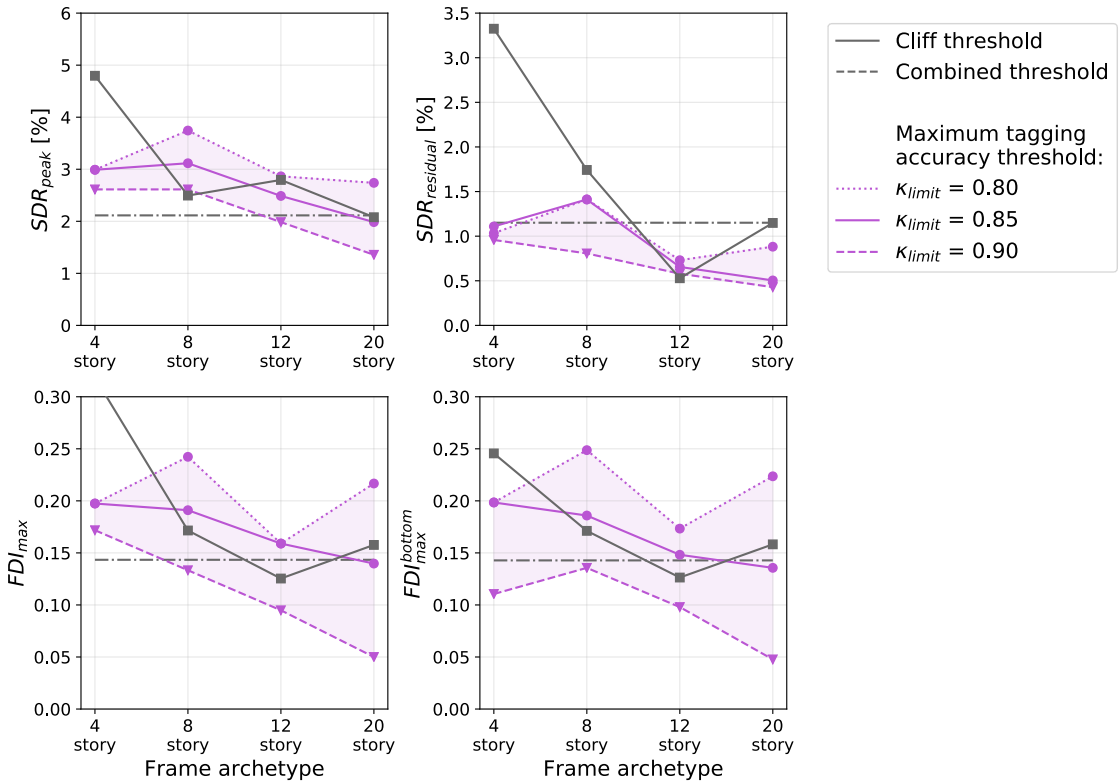

FIGURE 11 Alternative safety thresholds for **(a)** SDR_{peak}, **(b)** $SDR_{residual}$, **(c)** DI_{hinges}, **(d)** FDI_{max} and **(e)** DI_{sdr} for the four ductilre RC frame archetypes.

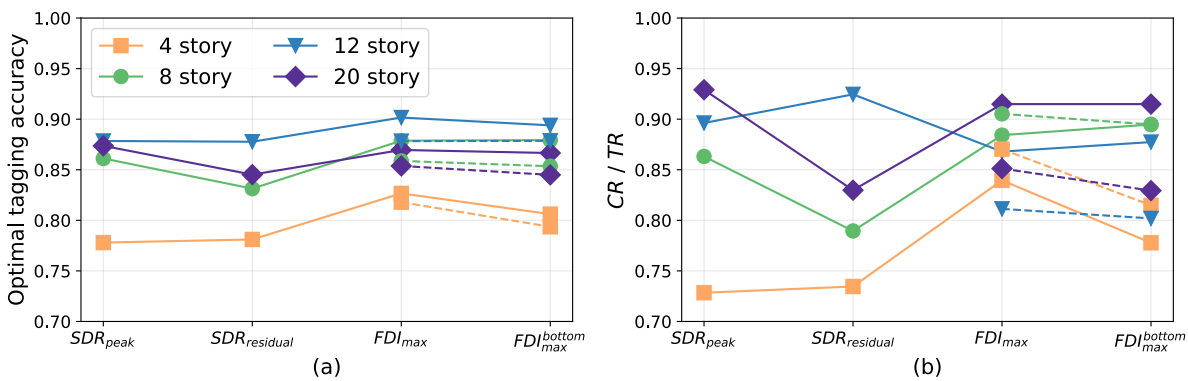

FIGURE 12 Summary of statistics on tagging accuracy **(a)** Optimal tagging accuracy; and **(b)** Fraction of correctly classified red tags for the candidate damage indicators and each building archetype considering κ_{limit}=0.85 for accuracy calculations. Continuous lines show the maximum accuracy thresholds, while dashed lines represent the recommended damage indicators and threshold criteria presented in Section 4.6

4.6 | Recommend safety criteria for the structure

The previous subsections demonstrate that FDI_{max} and FDI_{max}^{bottom} are the most efficient and robust of the considered damage indicators for RC buildings. Based on observations from Figure 11, we propose a constant safety threshold for both FDI_{max} and FDI_{max}^{bottom} = 0.17. These values imply that all beam hinges of the critical floor have DS1 (numerous residual cracks, width≥0.06in, extending one section depth from the element end).

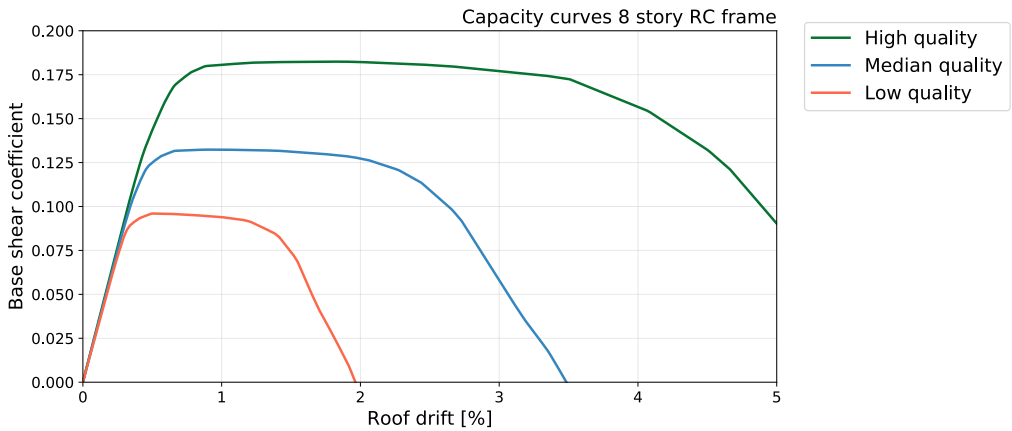

FIGURE 13 Pushover curve for the 8-story archetype with low, median, and high-quality material properties using a uniform lateral load pattern.

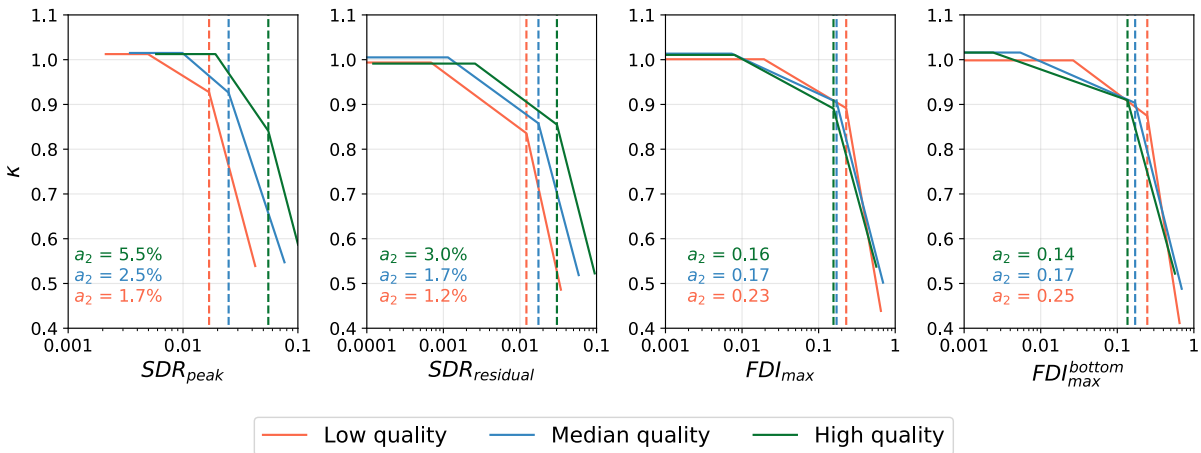

FIGURE 14 Comparison of tri-linear parametric model for the 8-story archetype with low, median, and high structural component model parameters for SDR_{peak}, $SDR_{residual}$, FDI_{max}, and FDI_{max}^{bottom}.

The generalized safety criterion does not significantly reduce the optimal tagging accuracy as depicted by the dashed lines in Figure 12. As expected, FDI_{max} performs better than FDI_{max}^{bottom} because it captures the rare cases where the worst floors are in the upper three-quarters of the building. However, FDI_{max} requires careful inspection of all the floors of the building in order to identify the worst. FDI_{max}^{bottom} offers a more practical alternative that performs almost as well but reduces the number of floors that need to be inspected to only the bottom quarter of the building. We can further reduce the amount of inspection required by defining a minimum amount of beams to inspect per floor to have a reliable estimation of the FDI. But such refinement is outside the scope of this paper. The recommended safety criteria are not limited to field applications, but can also be used to expedite post-earthquake risk modeling of existing structures without computationally expensive sequential IDAs. The analyst would only need to estimate the value of the damage indicator of the structure for a representative suite of damaging ground motion and compute the damage indicator for each record. The likelihood that the structure is unsafe can be estimated as the fraction of damaging earthquakes that produce a damage indicator larger than the threshold of the recommended safety criteria.

5 | SUMMARY AND CONCLUSIONS

In this paper, we propose a methodology that uses simulation results to identify relevant damage indicators and associated safety thresholds for determining whether a damaged structure is safe to occupy. This methodology enables the development of more accurate safety guidelines that augment current post-earthquake evaluation criteria and help identify structures that need to be evacuated. The simulation-based methodology provides a path to develop safety guidelines for any structural system, even for those that have not yet been observed in strong earthquakes.

The proposed methodology has five steps. The first step fits a trilinear model to predict median collapse capacity as a function of each candidate damage indicator. The second step uses the fitting error of the trilinear models to measure the prediction efficiency of each damage indicator. The damage indicators with the highest fitting errors should be discarded. The third step identifies the optimal threshold for each damage indicator, based on a metric of accuracy in categorizing whether the structure's performance has reduced beyond a given limit for median collapse capacity. The fourth step assesses the robustness of the safety thresholds to model uncertainty using a sensitivity approach. The damage indicators with thresholds that change significantly due to modeling uncertainty should be discarded. The fifth step uses the remaining damage indicators and their optimal thresholds to recommend quantitative safety criteria for a particular structural type. The collapse fragilities for damaged structures can be computed as an optional sixth step.

The capabilities of this methodology are demonstrated with a case study of ductile RC frame buildings. The case study considers damage indicators based on drift, ground motion intensity, fractions of damaged components, and floor damage indices. The latter takes beam and column hinge damage on a floor-by-floor basis and combines them to produce floor damage indexes. For the case study, floor damage indexes are the only type of damage indicators that have all of the following characteristics: (1) are the most efficient in predicting the collapse safety of damaged buildings; (2) their safety thresholds tend to be constant regardless of the number of stories which facilitates the selection of general recommendations for tagging RC buildings; and (3) are robust to modeling uncertainty. The recommended safety criterion labels a ductile RC frame building as unsafe when all beam hinges of the critical floor have numerous residual cracks extending at least one section depth from the face of the column. This safety criterion has a level of accuracy of approximately 80% when compared to directly tagging damaged buildings based on their reduction in collapse capacity. The recommended safety criteria are not limited to field applications, but can also be used to expedite post-earthquake risk modeling of existing structures without computationally expensive sequential IDAs.

Although the case study in this paper considered RC buildings, the simulation-based methodology proposed can be applied to any structure type to identify specific damage indicators and their corresponding thresholds. For instance, the number of fractured beam-to-column connections or the damage to column splices may be good candidate damage indicators for steel moment frame buildings. Similarly, the damage state of structural walls and spandrel beams could be good candidates for RC wall buildings. The computational effort to develop thresholds for new systems is significant yet commensurate with the resources typically available at research institutions. The application of these thresholds in a post-earthquake setting would not require additional sequential IDAs by the analyst. Taking a broader perspective, the application of this methodology to other types of structures can inform the future post-earthquake evaluation guidelines that focus on quantitative safety thresholds to reduce subjective judgment and increase confidence in safety decisions, even for difficult cases.

6 | SUPPORTING MATERIAL

The code that creates all the figures in this paper can be found in the following repository[48] with DOI: 10.5281/zenodo.7503565. The module with the supporting functions that implement all the calculations of damage indicators and post-processing is in the following repository: https://github.com/annehulsey/aftershock_analysis All the NLRHA results are available in DesignSafe[49] Data Depot[50] with DOI: 10.17603/ds2-3d7j-7w80.

7 | ACKNOWLEDGMENTS

This research was supported by the National Institute of Standards and Technology (NIST Award 70NANB17H245), a Fulbright-Colciencias grant, a graduate fellowship from FEMA, the Blume Earthquake Engineering Center, the Stanford Research Computing Center, and Stanford University. The authors also acknowledge Jill O'Nan, Carlos Molina Hutt, Rodrigo Silva-Lopez, Amory Martin, Kuanshi Zhong, Emily Mongold, and Andy Ziccarelly for their constructive comments on this manuscript.

Some of the computing for this project was performed on the Sherlock cluster. We would like to thank Stanford University and the Stanford Research Computing Center for providing computational resources and support that contributed to these research results.

References

1. ATC-20-1 . Field Manual: Postearthquake Safety Evaluations of Buildings (2nd Edition). tech. rep., Applied Technology Council; Redwood City, CA: 2005.

2. AMVA , Uniandes . Guía de Evaluación de Daños en Edificaciones después de un Desastre. tech. rep., Universidad de los Andes; Área Metropolitana del Valle de Aburrá: 2018.

3. Marshall JD, Jaiswal K, Gould N, Turner F, Lizundia B, Barnes JC. Post-earthquake building safety inspection: Lessons from the canterbury, New Zealand, earthquakes. *Earthquake Spectra* 2013; 29(3): 1091–1107. doi: 10.1193/1.4000151

4. FEMA . Evaluation of earthquake damaged concrete and masonry wall buildings - FEMA 306. tech. rep., Applied Technology Council; Redwood City, CA: 1998.

5. FEMA . Recommended postearthquake evaluation and repair criteria for welded steel moment-frame buildings, SAC Joint Venture-FEMA-352. 2000.

6. Bazzurro P, Cornell CA, Menun C, Motahari M. Guidelines For Seismic Assessment Of Damaged Buildings. *13th World Conference on Earthquake Engineering* 2004: No. 1708.

7. Luco N, Bazzurro P, Cornell CA. Dynamic Versus Static Computation Of The Residual Capacity Of A Mainshock-damaged Building To Withstand An Aftershock. *13th World Conference on Earthquake Engineering* 2004: No. 2405.

8. Maffei JR, Telleen K, Nakayama Y. Probability-based seismic assessment of buildings, considering post-earthquake safety. *Earthquake Spectra* 2008; 24(3): 667–699. doi: 10.1193/1.2950066ÍŤ

9. Iervolino I, Chioccarelli E, Suzuki A. Seismic damage accumulation in multiple mainshock-aftershock sequences. *Earthquake Engineering and Structural Dynamics* 2020(August 2019): 1–21. doi: 10.1002/eqe.3275

10. Ruiz-García J, Chora C. Evaluation of approximate methods to estimate residual drift demands in steel framed buildings. *Earthquake Engineering Structural Dynamics* 2015; 44(15): 2837–2854. doi: 10.1002/eqe.2611

11. Raghunandan M, Liel AB, Luco N. Aftershock collapse vulnerability assessment of reinforced concrete frame structures. *Earthquake Engineering Structural Dynamics* 2015; 44(3): 419–439. doi: 10.1002/eqe.2478

12. Burton HV, Sreekumar S, Sharma M, Sun H. Estimating aftershock collapse vulnerability using mainshock intensity, structural response and physical damage indicators. *Structural Safety* 2017. doi: 10.1016/j.strusafe.2017.05.009

13. Zhang Y, Burton HV. Pattern recognition approach to assess the residual structural capacity of damaged tall buildings. *Structural Safety* 2019; 78: 12–22. doi: 10.1016/J.STRUSAFE.2018.12.004

14. Li Y, Song R, Van De Lindt JW. Collapse fragility of steel structures subjected to earthquake mainshock-aftershock sequences. *Journal of Structural Engineering (United States)* 2014; 140(12): 1–10. doi: 10.1061/(ASCE)ST.1943-541X.0001019

15. Burton HV, Deierlein GG. Integrating visual damage simulation, virtual inspection, and collapse capacity to evaluate post-earthquake structural safety of buildings. *Earthquake Engineering Structural Dynamics* 2018; 47(2): 294–310. doi: 10.1002/eqe.2951

16. Zhang Y, Burton HV, Shokrabadi M, Wallace JW. Seismic risk assessment of a 42-story reinforced concrete dual-system building considering mainshock and aftershock hazard. *Journal of Structural Engineering* 2019; 145(11): 04019135. doi: 10.1061/(ASCE)ST.1943-541X.0002427

17. Zhang Y, Burton HV, Sun H, Shokrabadi M. A machine learning framework for assessing post-earthquake structural safety. *Structural Safety* 2018; 72: 1–16. doi: 10.1016/j.strusafe.2017.12.001

18. Gokkaya BU, Baker JW, Deierlein GG. Estimation and impacts of model parameter correlation for seismic performance assessment of reinforced concrete structures. *Structural Safety* 2017; 69: 68–78. doi: 10.1016/j.strusafe.2017.07.005

19. Ruiz-García J, Aguilar JD. Aftershock seismic assessment taking into account postmainshock residual drifts. *Earthquake Engineering Structural Dynamics* 2015; 44(9): 1391–1407. doi: 10.1002/eqe.2523

20. Vamvatsikos D, Cornell CA. Incremental dynamic analysis. *Earthquake Engineering Structural Dynamics* 2002; 31(3): 491–514. doi: 10.1002/eqe.141

21. FEMA . Quantification of building seismic performance factors - FEMA P695. tech. rep., Applied Technology Council; Redwood City: 2009.

22. Jeon JS, DesRoches R, Lowes LN, Brilakis I. Framework of aftershock fragility assessment-case studies: older California reinforced concrete building frames. *Earthquake Engineering Structural Dynamics* 2015; 44(15): 2617–2636. doi: 10.1002/eqe.2599

23. Mitrani-reiser J. *An ounce of prevention: Probabilistic loss estimation for performance-based earthquake engineering*. PhD thesis. California Institute of Technology, Pasadena, California; 2007.

24. Mitrani-Resier J, Wu S, Beck JL. Virtual Inspector and its application to immediate pre-event and post-event earthquake loss and safety assessment of buildings. *Natural Hazards* 2016; 81(3): 1861–1878. doi: 10.1007/s11069-016-2159-6

25. Moehle J, Deierlein GG. A framework methodology for performance-based earthquake engineering. *13th World Conference on Earthquake Engineering* 2004: No. 679.

26. FEMA . Seismic performance assessment of buildings FEMA P-58. Tech. Rep. September, Applied Technology Council; Washington, D.C.: 2012.

27. Miranda E. Use of probability-based measures for automated damage assessment. *The Structural Design of Tall and Special Buildings* 2006; 15(1): 35–50. doi: 10.1002/tal.342

28. Baker JW, Cornell AC. Spectral shape, epsilon and record selection. *Earthquake Engineering and Structural Dynamics* 2006; 35(9): 1077–1095. doi: 10.1002/eqe.571

29. Eads L, Miranda E, Lignos DG. Average spectral acceleration as an intensity measure for collapse risk assessment. *Earthquake Engineering Structural Dynamics* 2015; 44(12): 2057–2073. doi: 10.1002/eqe.2575

30. Cordova PP, Deierlein GG, Mehanny SS, Cornell C. Development of a two-parameter seismic intensity measure and probabilistic assessment procedure. In: No. January. ; 2000.

31. Bianchini M, Diotallevi P, Baker JW. Prediction of inelastic structural response using an average of spectral accelerations. *10th international conference on structural safety and reliability (ICOSSAR09)* 2009: 8.

32. Kohrangi M, Kotha SR, Bazzurro P. Ground-motion models for average spectral acceleration in a period range: direct and indirect methods. *Bulletin of Earthquake Engineering* 2018; 16(1): 45–65. doi: 10.1007/s10518-017-0216-5

33. Ryu H, Luco N, Uma SR, Liel AB. Developing fragilities for mainshock-damaged structures through incremental dynamic analysis. *Proceedings of the Ninth Pacific Conference on Earthquake Engineering* 2011.

34. Magnani A, Boyd SP. Convex piecewise-linear fitting. *Optimization and Engineering* 2009; 10(1): 1–17. doi: 10.1007/s11081-008-9045-3

35. Luco N, Cornell CA. Structure-specific scalar intensity measures for near-source and ordinary earthquake ground motions. *Earthquake Spectra* 2007; 23(2): 357–392. doi: 10.1193/1.2723158

36. Hastie T, Tibshirani R, Friedman J. *The elements of statistical learning*. Springer Series in Statistics. 2nd ed. 2009

37. Hulsey AM, Galvis FA, Baker JW, Deierlein GG. Graphically Communicating the Risk of Building Collapse due to Aftershock Hazard and Post-Earthquake Damage. *12 National Conference of Earthquake Engineering* 2022.

38. ASCE/SEI 7-16 . *Minimum Design Loads and Associated Criteria for Buildings and Other Structures*. Reston, VA: American Society of Civil Engineers. 7-16 ed. 2016

39. ACI 318-14 . *Building Code Requirements for Structural Concrete (ACI 318-14)*. 11. Farmington Hills, MI: American Concrete Institute . 2014.

40. Haselton CB, Deierlein GG. Assessing seismic collapse safety of modern reinforced concrete moment-frame buildings, PEER Report 2007/08. Tech. Rep. February, Pacific Earthquake Engineering Research Center; Berkeley, CA: 2008

41. McKenna F. OpenSees: A framework for earthquake engineering simulation. *Computing in Science and Engineering* 2011; 13(4): 58–66. doi: 10.1109/MCSE.2011.66

42. Ibarra LF, Medina RA, Krawinkler H. Hysteretic models that incorporate strength and stiffness deterioration. *Earthquake Engineering and Structural Dynamics* 2005; 34(12): 1489–1511. doi: 10.1002/eqe.495

43. Haselton CB, Liel AB, Taylor-Lange SC, Deierlein GG. Calibration of model to simulate response of reinforced concrete beam-columns to collapse. *ACI Structural Journal* 2016; 113(6): 1141–1152. doi: 10.14359/51689245

44. Altoontash A. *Simulation and damage models for performance assessment of reinforced concrete beam-column joints*. PhD thesis. Stanford University, Stanford, CA; 2004.

45. Harrington CC, Liel AB. Collapse assessment of moment frame buildings, considering vertical ground shaking. *Earthquake Engineering Structural Dynamics* 2016; 45(15): 2475–2493. doi: 10.1002/eqe.2776

46. Haselton CB, Deierlein GG, Liel AB, Dean BS, Chou JH. Seismic Collapse Safety of Reinforced Concrete Buildings. I: Assessment of Ductile Moment Frames. *Journal of Structural Engineering* 2011; 137(4): 481–491. doi: 10.1061/(ASCE)ST.1943-541X.0000318.

47. Ramirez CM, Miranda E. Significance of residual drifts in building earthquake loss estimation. *Earthquake Engineering Structural Dynamics* 2012; 41(11): 1477–1493. doi: 10.1002/eqe.2217

48. Galvis FA, Hulsey AM. DamageIndicators EESD v0: Code to generate the figures in the damage indicator paper. *Zenodo* 2023. doi: DOI: 10.5281/zenodo.7503565

49. Rathje EM, Dawson C, Padgett JE, et al. DesignSafe: New Cyberinfrastructure for Natural Hazards Engineering. *Natural Hazards Review* 2017; 18(3): 06017001. doi: 10.1061/(asce)nh.1527-6996.0000246

50. Galvis FA, Hulsey AM, Deierlein GG, Baker JW. Damaged simulations of RC frames. *DesignSafe Data Depot* 2023. doi: 10.17603/ds2-3d7j-7w80

How to cite this article: [1]Galvis F. A., [2]Hulsey A. M, [3]Baker J. W. and [3]Deierlein G. G. (2022), Simulation-Based Methodology to Identify Damage Indicators and Safety Thresholds for Post-Earthquake Evaluation of Structures, *Earthquake Engng Struct Dyn*, *202X;00:X–X*.